Correspondence to:
J. Li,
jun.li@ssec.wisc.edu

ABI Water Vapor Radiance Assimilation in a Regional NWP Model by Accounting for the Surface Impact

Jung-Rim Lee[1] [iD] , **Jun Li[2]** [iD] , **Zhenglong Li[2]** [iD] , **Pei Wang[2]** [iD] , and **Jinlong Li[2]**

[1]Korea Meteorological Administration, Seoul, South Korea, [2]Cooperative Institute for Meteorological Satellite Studies, University of Wisconsin-Madison, Madison, WI, USA

Abstract There are a growing number of advanced imagers for geostationary meteorological satellites, which can provide water vapor radiance observations with high temporal and spatial resolutions. To assess the impact of those imagers, radiance assimilation experiments were conducted with the Advanced Baseline imager (ABI) on board the Geostationary Operational Environmental Satellite-16. The radiances from the three water vapor absorption bands of Geostationary Operational Environmental Satellite-16 ABI were assimilated through the National Oceanic and Atmospheric Administration Gridpoint Statistical Interpolation data assimilation system in a regional numerical weather prediction (NWP) model. The forecast impacts for Hurricane Irma (2017) and Hurricane Harvey (2017) have been studied and analyzed in this work. Due to complicated surface situations (emissivity, terrain height, etc.) over land, the infrared (IR) radiance assimilation is still limited; thus, handling surface effects in radiance assimilation needs to be considered. By analyzing the Jacobian function of skin temperature in the ABI radiance assimilation process, it is shown that assimilating water vapor IR radiances over high elevation surfaces or in dry regions is problematic even where the bands are mostly sensitive to the upper level of the atmosphere such as Band 8 (6.19 μm). Additional quality control steps using skin temperature Jacobians to eliminate the contamination from the surface impact are developed and added for ABI radiance assimilation. The results show that ABI radiance assimilation with quality controls is able to improve tropical cyclone forecasts. The methodology used in this study can be applied to the assimilation of IR radiances from other geostationary satellites or polar-orbiting satellites.

1. Introduction

Advanced imagers such as the Advanced Baseline Imager (ABI; Schmit et al., 2005, 2017) on board the Geostationary Operational Environmental Satellites (GOES)-16 and GOES-17, the Advanced Himawari Imager (AHI) on board Himawari-8 (H8) and H9, the Advanced Meteorological Imager on board GEO-KOMPSAT 2A, and the Advanced Geosynchronous Radiation Imager on board FengYun-4A (Min et al., 2017; Yang et al., 2017) can provide observations with high temporal (1- to 15-min) and high spatial (0.5- to 2-km) resolutions at 14–16 bands ranging for visible to infrared (IR) spectral regions. These observations can help monitor, understand, and predict high-impact weather events such as tropical cyclones (TCs). One important application of geostationary satellite data is to improve weather forecasts by assimilating the observations into numerical weather prediction (NWP) models, especially when information from three water vapor absorption bands is included.

Assimilating geostationary satellite data has shown positive impacts in both global and regional NWP models. Coastal precipitation forecasts are improved with direct assimilation of GOES-11 and GOES-12 IR radiances (Qin et al., 2013; Zou et al., 2011). Moreover, assimilating 10 AHI/H8 IR channels showed better performance than using the four inherited channels from the previous generation of geostationary satellites, such as the Communication, Ocean and Meteorological Satellite (COMS), the multifunctional transport satellite-2, and GOES-15 (Qin et al., 2017). Water vapor information from AHI, such as layered precipitable water retrievals and the radiances themselves, were also tested in a regional NWP model. This has shown improvement in rainfall forecast amounts (Wang et al., 2018), especially when combined with appropriate cumulus and microphysical parameterization schemes (Lu et al., 2019). AHI/H8 data have also been assimilated in the Global Forecast System (GFS) and have shown that IR water vapor channels reduce the analysis and forecast errors in upper-tropospheric humidity (Ma et al., 2017).

Table 1
ABI Bands and Characterizations

Band	Central wavelength (μm)	Subpoint pixel spacing (km)	Descriptive name
1	0.47	1	Blue
2	0.64	0.5	Red
3	0.864	1	Vegetation
4	1.373	2	Cirrus
5	1.61	1	Snow/ice
6	2.24	2	Cloud particle size
7	3.90	2	Shortwave window
8	6.19	2	Upper-level water vapor
9	6.93	2	Midlevel-level water vapor
10	7.34	2	Lower-level water vapor
11	8.44	2	Cloud-top phase
12	9.61	2	Ozone
13	10.33	2	Clean longwave window
14	11.21	2	Longwave window
15	12.29	2	Dirty longwave window
16	13.28	2	CO_2

Note. Bands 8, 9, and 10 (in italics) radiances are assimilated in this study. ABI = Advanced Baseline imager.

The GOES-16 ABI imager was launched on 19 November 2016. ABI is a 16-band radiometer (Table 1) covering the visible (Bands 1–3; 0.47, 0.64, and 0.864 μm), near-IR (Bands 4–6; 1.373, 1.61, and 2.24 μm), and IR (Bands 7–16; 3.90, 6.19, 6.93, 7.34, 8.44, 9.61, 10.33, 11.21, 12.29, and 13.28 μm) regions. The ABI can simultaneously scan 16 spectral bands to produce a full disk every 10 min and allows for rapid scan and contiguous U.S. imaging automatically interleaved with full disk scanning. The spatial resolution of the ABI bands are 0.5 km (Band 2), 1 km (Bands 1, 3, and 5), and 2 km (Bands 4 and 11 IR bands) at nadir. The ABI observed imagery is widely used in monitoring weather and the environment, such as severe local storms, TCs and hurricanes, aviation, natural hazards, land and ocean surfaces, and the cryosphere. In addition, ABI information is used to produce a wide variety of weather and environmental data products that can be assimilated in NWP models.

In this study, we focus on how to better use the three water vapor bands' radiances to improve TC forecasts. A basic description of the ABI water vapor bands, data assimilation system and forecast model, and selected TC cases is given in section 2. Section 3 is an overview of the experiment design and the initial results of ABI radiance assimilation. In section 4, the surface impact of ABI radiances assimilation is investigated. Also, additional experiments to deal with the surface effects are explained, and the model forecast impact results are presented. A summary of findings follows in section 5.

2. Background

2.1. ABI Radiance Measurements

The ABI channels and characterizations are described in Table 1. Three water vapor bands (8, 9, and 10) are most sensitive from lower to upper-level humidity in the troposphere (Schmit et al., 2005), which provide information on vertical moisture profiles. The Jacobian functions in Figure 1 show the sensitivities of ABI radiances to the temperature and moisture profiles for the three ABI water vapor bands. Band 8 (6.19 μm), peaks highest in the vertical, around 367 hPa for temperature. Band 9 (6.93 μm) and Band 10 (7.34 μm) peak around 450 and 650 hPa for temperature, respectively, with a U.S. standard atmosphere. The peak levels of the water vapor Jacobian functions are slightly higher than the temperature Jacobian functions showing 351, 399, and 545 hPa for the three water vapor bands. The 6.19- and 6.93-μm bands contain information about high- and middle-level atmospheric water vapor. The information from two bands can be used for jet stream identification, severe weather analysis, estimation of upper-level moisture, and atmospheric motion vectors. In addition, the information can help to forecast hurricane track and severe weather when assimilating it into an NWP model (Moody et al., 1999; Soden & Bretherton, 1993; Weldon & Holmes, 1991). The 7.34-μm band is sensitive to middle- and lower-level atmospheric flow and can help identify jet streaks. It is also sensitive to SO_2 and can be used to identify and track volcanic plumes (Realmuto et al., 1997).

2.2. Data Assimilation and Modeling Systems
2.2.1. Data Assimilation System
All data assimilations were conducted using the Community Gridpoint Statistical Interpolation (GSI) system version 3.6 from the Developmental Testbed Center. GSI is a unified data assimilation system for both global and regional applications and is currently capable of two-dimensional variational analysis (2DVar), 3DVar, 3-D/4-D ensemble-variational (EnVar), 3-D/4-D hybrid EnVar, or 4DVar (Hu et al., 2017). The types of observations GSI can assimilate vary from conventional data to aerosol observations including most satellite data. However, at the time of this writing, GSI version 3.6 did not allow the ingestion and processing of ABI radiances; thus, some modules are implemented in this study. Newly added modules are created with reference to the AHI radiance assimilation modules in the GSI version 3.6. For cloud detection, a clear-sky filter using a split-window surface temperature test versus forecast
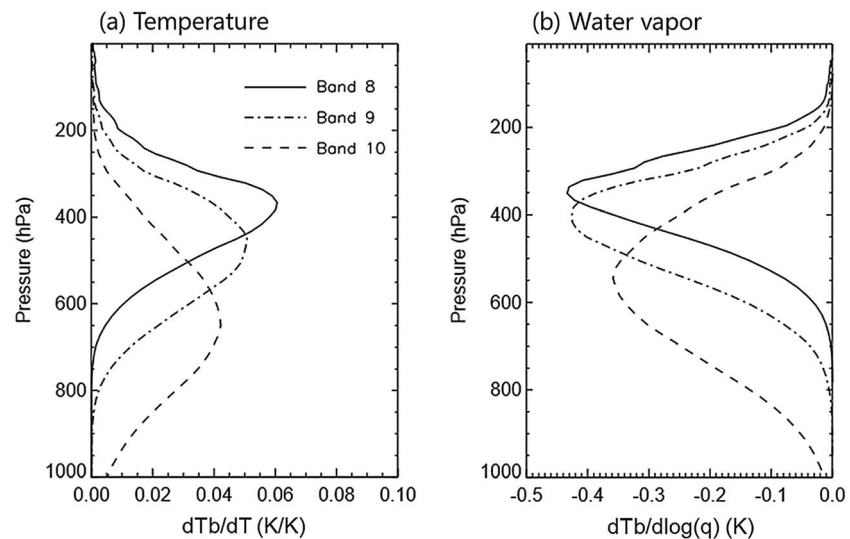
Figure 1. The Jacobian functions of Advanced Baseline imager Bands 8, 9, and 10 calculated with Community Radiative Transfer Model for the U.S. standard atmosphere, 1976. (a) Temperature. (b) Water vapor.

background is applied (Ma et al., 2017). The Community Radiative Transfer Model (CRTM) developed by the Joint Center for Satellite Data Assimilation is embedded as the fast radiative transfer model in GSI (Chen et al., 2010, 2012) to provide forward and Jacobian calculations. The CRTM coefficients Version 2.2.3 were used in the GSI.

2.2.2. Forecast Model

The Weather Research and Forecasting (WRF) model, version 3.6.1, was used with the Advanced Research WRF (ARW) model dynamical core. WRF-ARW is a mesoscale NWP system designed for both atmospheric research and operational forecasting applications (Skamarock et al., 2008). The ARW is a nonhydrostatic Eulerian dynamical core with terrain-following, pressure-based vertical coordinates and can be used for a broad range of applications across scales ranging from tens of meters to thousands of kilometers. The WRF-ARW has been developed, and maintained, primarily by NCAR's Mesoscale and Microscale Meteorology Laboratory. For the simulation, the WRF single-moment, six-class microphysics scheme (Hong & Lim, 2006), the Kain-Fritsch cumulus parameterization scheme (Kain, 2004), and the Yonsei University planetary boundary layer scheme (Hong et al., 2006) were selected. The Rapid Radiative Transfer Model for global applications scheme (Iacono et al., 2008) was utilized as the longwave and shortwave radiation scheme.

2.2.3. TC Cases for Impact Studies

Two 2017 Atlantic TCs were selected to study the impacts of ABI radiance assimilation: Hurricanes Irma and Harvey. Hurricane Harvey (2017) initially started as a typical weak August tropical storm and dissipated over the central Caribbean Sea. However, after reforming over the Bay of Campeche, Harvey rapidly intensified into a Category 4 hurricane before making landfall along the middle Texas coast. The storm then stalled for 4 days, dropping historic amounts of rainfall of more than 150 centimeters over southeastern Texas. These rains caused catastrophic flooding making Harvey the second costliest hurricane in U.S. history, behind Katrina (2005; Blake & Zelinsky, 2018). Property losses from Harvey were assessed at $125 billion, and there were 68 fatalities.

Hurricane Irma (2017) was a long-lived hurricane that reached Category 5 intensity on the Saffir-Simpson Hurricane Wind Scale. The catastrophic hurricane made seven landfalls, four of which occurred as a Category 5 hurricane across the northern Caribbean Islands. Irma made landfall as a Category 4 hurricane in the Florida Keys and struck southwestern Florida at Category 3 intensity. Irma caused widespread devastation across the affected areas and was one of the strongest and costliest hurricanes on record in the Atlantic Basin (Cangialosi et al., 2018).

3. Data, Experiments, and the Impact Studies

3.1. Data and Experiments

The National Centers for Environmental Prediction operational GFS final reanalysis data (FNL) were employed as initial and boundary conditions for the experiments. The original grid size of the data was 1° by 1°. It was interpolated to the model grid both horizontally and vertically for the TC simulations. The horizontal grid size for the simulation was 12 km, and the vertical range was from the surface to 10 hPa with 51 levels. At the beginning of the simulation, the initial condition was generated using the GFS analysis. Cycling data assimilation was then conducted every 6 hr to update the first guess, and the boundary condition was updated as well. Following each analysis, the WRF model simulated 120-hr forecasts for Hurricane Irma and 72-hr forecasts for Hurricane Harvey.

All experiments assimilated conventional observation data from the World Meteorological Organization's Global Telecommunication System including radiosondes, wind profilers, aircraft data, and surface observations. Moreover, radiances from polar orbiting satellites were assimilated, including from the Advanced Microwave Sounding Unit (AMSU-A) on NOAA-15/-18/-19; the AMSU-A and the Infrared Atmospheric Sounding Interferometer (IASI) on Metop-A/-B; and the Cross-track Infrared Sounder (CrIS), clear only, the CrIS Cloud-Cleared radiances (CCRs), and the Advanced Technology Microwave Sounder (ATMS) on Suomi-NPP. The CrIS CCRs are an additional product to take advantage of the thermodynamic information from cloudy skies (Li et al., 2005, 2016; Wang et al., 2014). They are produced by the Cooperative Institute for Meteorological Satellite Studies at the University of Wisconsin-Madison. Wang et al. (2015, 2017) has shown that assimilating these data improves hurricane forecast track. The thinning sizes of the polar orbiting radiances are 120 km for IASI, CrIS, and ATMS and 60 km for AMSU-A. The bias correction coefficients for the polar orbiting radiances are preliminarily optimized (spun-up from GFS for 3 days before the hurricane forecast). Coefficients were updated at every assimilation cycle using the enhanced bias correction method in GSI (Zhu et al., 2014).

Two data assimilation experiments were conducted first to assess the overall impact of ABI radiances. In the control (CTL) run, conventional observations (CONV) and four types of polar orbiting radiances were assimilated in a 6-hr cycle. For the experiments (EXP), ABI radiances were assimilated on top of those assimilated in the CTL run. In the EXP, three water vapor bands (8, 9, and 10) were assimilated over both land and ocean (890_LS) with a thinning size of 30 km. First, the bias correction coefficients for the ABI radiance assimilation were carried out and updated at every assimilation cycle, similar to the process for the polar orbiting radiances.

1. CTL: CONV + AMSUA + ATMS + IASI + CrIS (including CCRs)
2. EXP (890_LS): CONV + AMSUA + ATMS + IASI + CrIS (including CCRs) + ABI

3.2. Hurricane Irma (2017)

A computational domain of the Hurricane Irma forecast in this study was centered at 70°W and 22°N with 450×370 horizontal grid points of 12-km resolution (green box in Figure 2). The experiments were initialized at 0600 UTC on 5 September 2017, with data assimilation starting at 1200 UTC on 5 September 2017 at 6-hr cycles followed by a 120-hr forecast. The cycle experiments were continued until 1800 UTC on 10 September 2017, with a total of 22 assimilation cycles for CTL and EXP.

Band 9 brightness temperature image and the data coverage of ABI radiances that were assimilated during the first analysis cycle (1200 UTC on 5 September 2017) are shown in Figures 3a and 3b, respectively. ABI radiances were assimilated only in clear sky regions, and the total number of radiances assimilated from the three water vapor bands was 33,970. The water vapor analysis differences between the CTL and EXP from the first analysis cycle are shown in Figures 3c–3e at three vertical levels (EXP − CTL). The assimilation of ABI water vapor radiances affects the moisture analysis field throughout the entire vertical level. The changes occur over the region where the radiances were assimilated and were most significant in the middle to upper levels of the troposphere with maximum changes of about 10% in the relative humidity. That is reasonable because the three water vapor bands peak in the middle to upper troposphere.

This study's forecast for Hurricane Irma (2017) along with the best track from the National Hurricane Center are shown in Figure 4 (890_JTs will be discussed in section 4). Based on the best track, Hurricane Irma
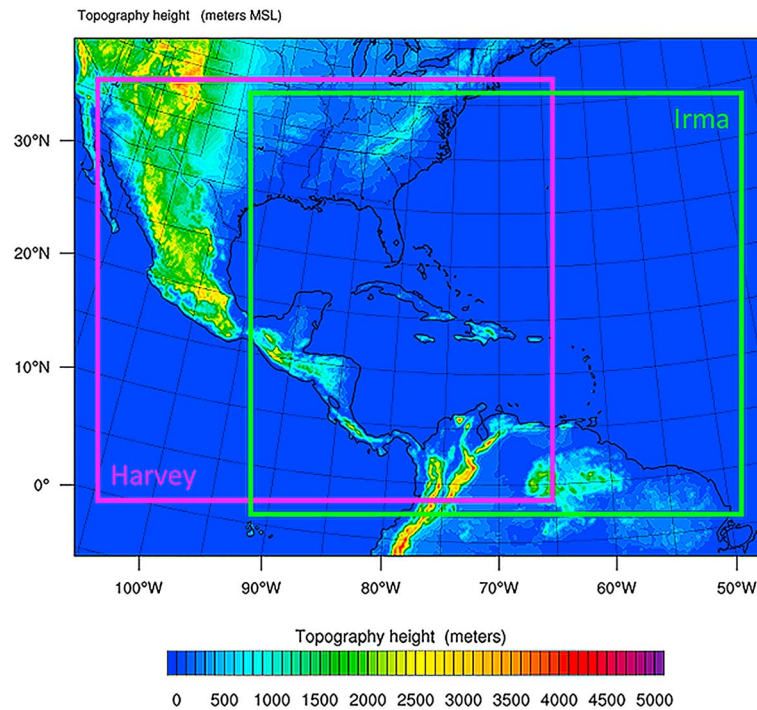
Figure 2. Computational domains of the Hurricane Irma (green box) and Hurricane Harvey (magenta box).

continued moving to the northwest west (NWW), then turned to the NNW near the Florida Keys, and passed through western Florida. However, the CTL predicted its landfall primarily in southeastern Florida and striking eastern Florida during the period of the experiment. Moreover, it predicted landfall in southeastern Georgia in the forecasts starting from 0000 UTC on 7 September 2017. The forecast track of
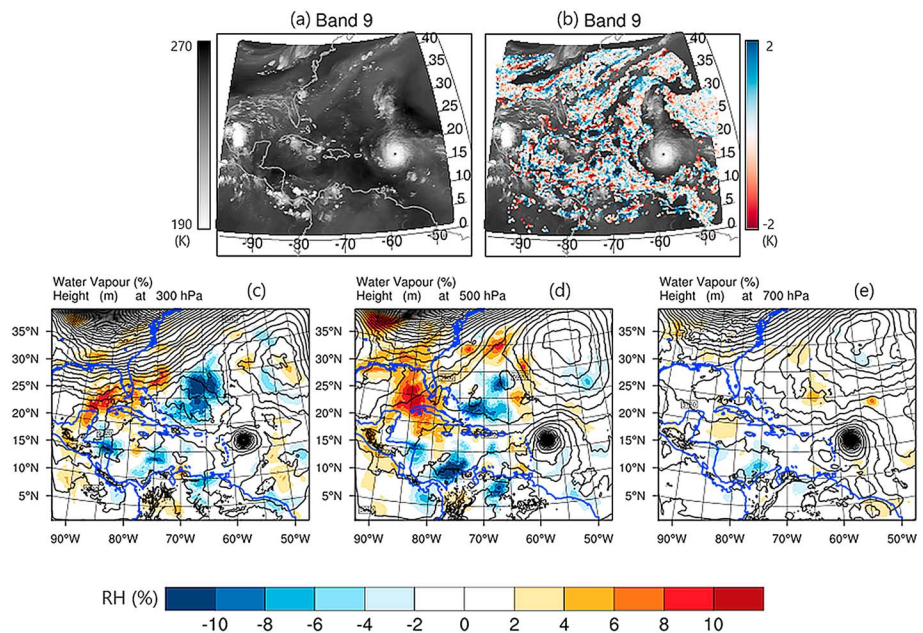

Figure 3. (a) GOES-16 ABI Band 9 image, (b) the same image as (a) with plots (bias-corrected observation minus analysis) assimilated ABI radiance at the first analysis time (1200 UTC on 5 September 2017); relative humidity analysis differences (EXP − CTL) at (c) 300 hPa, (d) 500 hPa, and (e) 700 hPa. ABI = Advanced Baseline imager; EXP = experiments; CTL = control run.
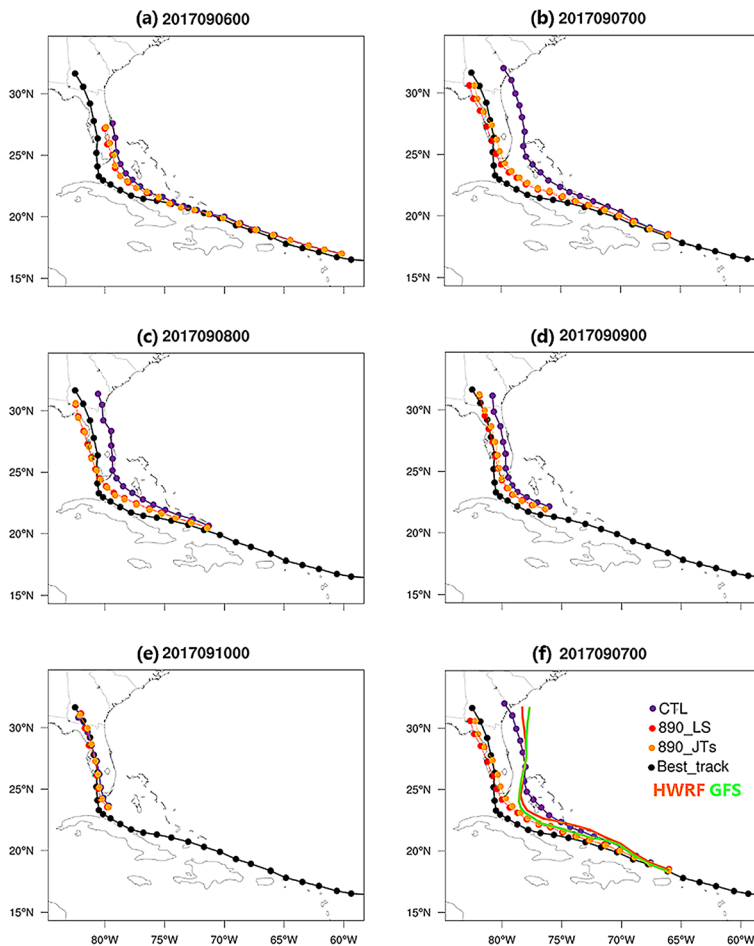
Figure 4. The Hurricane Irma forecast tracks from the different forecast time, and the best track (black). Each panels start forecast at (a) 2017090600, (b) 2017090700, (c) 2017090800, (d) 2017090900, (e) 2017091000, and (f) is same as (b), but added the forecast tracks from HWRF and GFS.CTL = control run; HWRF = Hurricane Weather Research and Forecasting.

the EXP of 890_LS indicated a more western landfall, and as a result, tracks are much closer to the best track. Hurricane Irma forecast differences between the CTL and EXP begin to emerge with the third cycle of this experiment (0000 UTC on 6 September 2017). It is clear that ABI radiance assimilation has a positive impact on track forecasting. The tendency, which pushes the forecast track to the west to be closer to the best track, is very consistent throughout the whole period in the EXP experiment. Finally, the forecasted tracks from the CTL and EXP converge with the best track starting from 0000 UTC on 10 September 2017.

For purposes of comparison, Figure 4f shows the operational forecast tracks from the GFS and the Hurricane WRF models produced by National Centers for Environmental Prediction not assimilating ABI radiances in their assimilation systems, overlapped with the forecasts from 0000 UTC on 7 September 2017 (Figure 4b). Both the GFS and Hurricane WRF models forecast the hurricane track better than the CTL until the hurricane turns northward, but after that, the tracks diverge from the best track making the difference much larger than the CTL. The Irma experiments indicate that the assimilation of ABI water vapor absorption band radiances help to improve the Hurricane Irma forecasts in terms of the hurricane track.

The forecast root-mean-square errors (RMSEs) of the hurricane track, maximum 10-m wind speed (MWS), and minimum sea level pressure (SLP) according to each forecast time are represented in Figure 5 (890_JTs will be discussed in section 4). The RMSEs are calculated using the reference track, MWS, and SLP from the National Hurricane Center's best track data set (Cangialosi et al., 2018). As expected from the hurricane track displays (in Figure 4), track forecast errors were substantially reduced with ABI radiance assimilation (890_LS) compared to the CTL at all forecast times (0–120 hr). In the 84-hr forecast, the track error (RMSE)
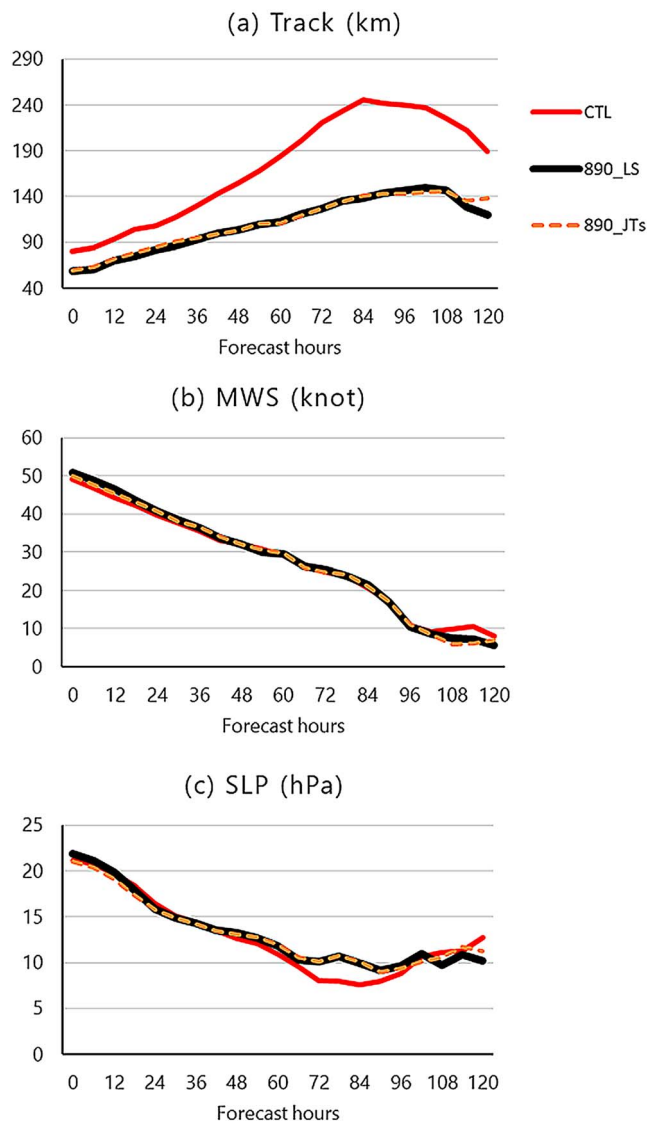
(a) Track (km)

(b) MWS (knot)

(c) SLP (hPa)

Figure 5. Root-mean-square errors of the (a) Hurricane Irma track, (b) MWS, and (c) SLP forecasts according to the forecast hours. CTL = control run; MWS = maximum 10-m wind speed; SLP = sea level pressure.

of Hurricane Irma was reduced up to 108 km. The MWS RMSEs did not show a big difference between the CTL and 890_LS but showed a slight positive impact after 96 hr. In the SLP, there were only slight differences until 48 hr, but the RMSEs of the 890_LS were slightly increased afterward and decreased again after 102 hr compared to the CTL.

To further investigate the changes of the atmospheric structures that led to improvement of the track forecasts, the temperature and geopotential height differences between the CTL and EXP of the forecasts at 0000 UTC on 7 September 2017 are displayed in Figure 6. The differences between the temperature fields at 300 hPa at the analysis time are less than 1 K (Figure 6a). The differences gradually increase with longer forecast times, resulting in temperature increases at the western edge of the hurricane center and temperature reduction across most of the hurricane center. The temperature difference is greater than 4 K for the 96-hr forecast. The changes in geopotential heights result from the temperature changes. Increasing geopotential heights over the east ocean of Florida from the 48- to the 96-hr forecast push the hurricane to the west so that it passes over the western part of Florida.

3.3. Hurricane Harvey (2017)

The center location of the domain for the Hurricane Harvey experiment was 87°W and 22°N with 400 × 370 grid points at 12-km resolution (magenta box in Figure 2). The experiments were initialized at 0000 UTC on 23 August 2017 with background from the FNL data, with data assimilation starting at 0600 UTC on 23 August 2017 until 1800 UTC on 25 August 2017 at 6-hr cycles (assimilating ABI radiance 15 times). Each analysis was followed by a 72-hr forecast. For the experiments, we set the forecast time at 72 hr, which differs from the Irma case (120 hr), due to its shorter lifespan.

The RMSEs of the hurricane track, MWS, and SLP before Hurricane Harvey made landfall were calculated to the best track data set from NHS (Blake & Zelinsky , 2018) and are shown in Figure 7 (890_JTs will be discussed in section 4). Results suggest that assimilating ABI radiances in the Harvey case show negative impacts in terms of both track and intensities (MWS and SLP). The hurricane track RMSEs are larger in the 890_LS until 42-hr forecast, and the RMSEs of the intensities are greater in the 890_LS than in the CTL. The departure of ABI radiances assimilated in the EXP is investigated in the following section in order to assess the reasons for negative impacts on Hurricane Harvey forecasts.

4. Handling Surface Impact for ABI Radiance Assimilation

4.1. Surface Impact of ABI Bands

Hurricane Harvey made its landfall over the middle Texas coast so that the computational domain of the Hurricane Harvey forecast in this study includes the southern United States and Central America, including the Rocky Mountains (in Figure 2). Because of that, more than one third of the domain is over land, and the highest surface altitude is about 4,000 m in Colombia and Venezuela. The high terrain may negatively impact the ABI water vapor radiance assimilation of Hurricane Harvey.

To assess the surface impact of ABI water vapor radiance assimilation on the Hurricane Harvey experiments, additional assimilation tests were carried out by changing ABI band use and land usage. Six simple tests were conducted assimilating ABI radiances at 0600 UTC on 23 August 2017 (the first cycle of the Hurricane Harvey experiments) as follows: Bands 8/9/10 over land and ocean (same as EXP); Band 8/9 over land and ocean (89_LS); Band 8 over land and ocean (8_LS); Bands 8/9/10 over ocean (890_S); Band 8/9 over
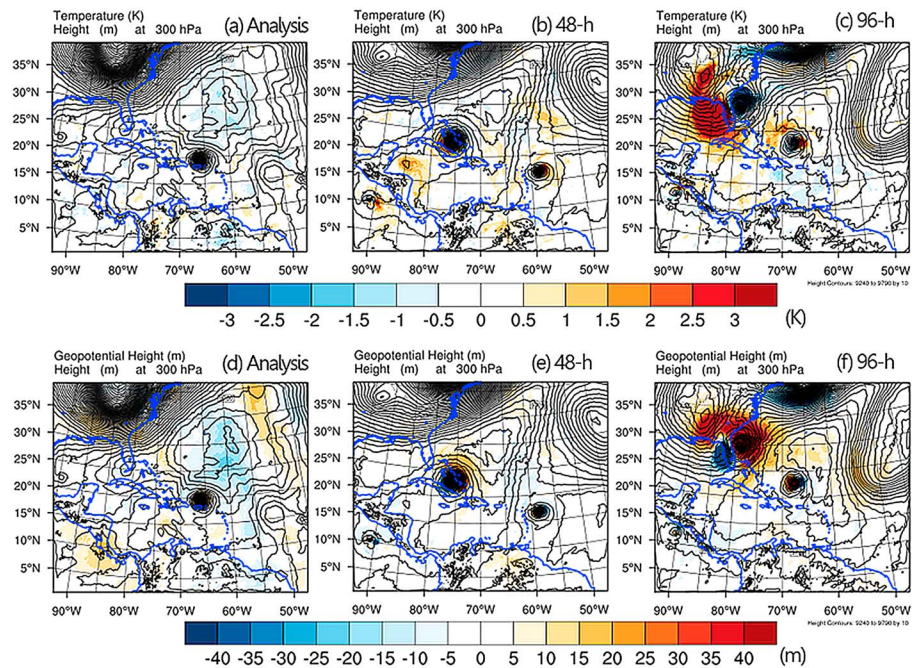
Figure 6. The temperature field differences of (a) the analysis, (b) 48-hr forecast, and (c) 96-hr forecast, and the geopotential height field difference of (d) the analysis, (e) 48-hr forecast, and (f) 96-hr forecast between the CTL and EXP (EXP − CTL) at 0000 UTC on 7 September 2017. CTL = control run; EXP = experiments.

ocean (89_S); and Band 8 over ocean (8_S). Then, the analysis difference (EXP − CTL) of relative humidity was calculated and displayed at three vertical levels (in Figure 8).

Overall impact of ABI radiance assimilation is strongest when the three water vapor bands are all assimilated over land and ocean (Figure 8a). The influences from ABI radiances are mostly concentrated in the middle to upper levels of the atmosphere, and the differences are decreased by eliminating Band 10 (Figure 8b) or Bands 9 and 10 (Figure 8c). It is also found that the regions with strong water vapor increase over Mexico and the Central America are coincident with their high surface terrain (Figure 2). The water vapor increment at 500 hPa is very strong in this region (Figure 8a). However, the increment weakens when removing Band 10 (at 500 hPa in Figure 8b). In Figure 8c, the increment almost disappeared when Bands 10 and 9 were removed (assimilate only Band 8).

Finally, the increment over high terrain also weakens by assimilating ABI radiances only over the ocean (Figures 8d–8f). These results indicate that there might be some limitations to assimilating ABI water vapor radiances over land for Hurricane Harvey.

4.2. Jacobian Function of Surface Skin Temperature

To investigate the surface impacts in the ABI radiance assimilation, the Jacobian function of surface skin temperature (J_{Ts}) was examined. The Jacobian function is the radiance response to a unit perturbation of the state variables, and it depends on the layer thickness. Here, Jacobian with respect to surface skin temperature ($\partial BT/\partial Ts$) was introduced to assess the direct change of radiances from the situational surface conditions. The values of J_{Ts} were extracted from the CRTM in GSI during the ABI radiance assimilation (890_LS).

Extracted J_{Ts} for the three water vapor absorption bands at 0600 UTC on 23 August 2017 are represented in Figure 9. Figures 9a–9c show the J_{Ts} when its value is greater than 0 K. A J_{Ts} greater than 0 indicates the radiance observation may see the surface. For this time period, there were 9,094 ABI Band 8 radiances assimilated, 546 of which had J_{Ts} above 0 K/K. Radiances were assimilated for Bands 9 and 10, 9,200 and 9,570, respectively, and all the J_{Ts} of the assimilated radiances have positive values. The plots of Band 8 J_{Ts} (Figure 9a) clearly show that Jacobian functions of surface skin temperature greater than 0 K/K are mainly seen over the high surface areas, such as the Rocky Mountains, Mexico, and Colombia. Over these
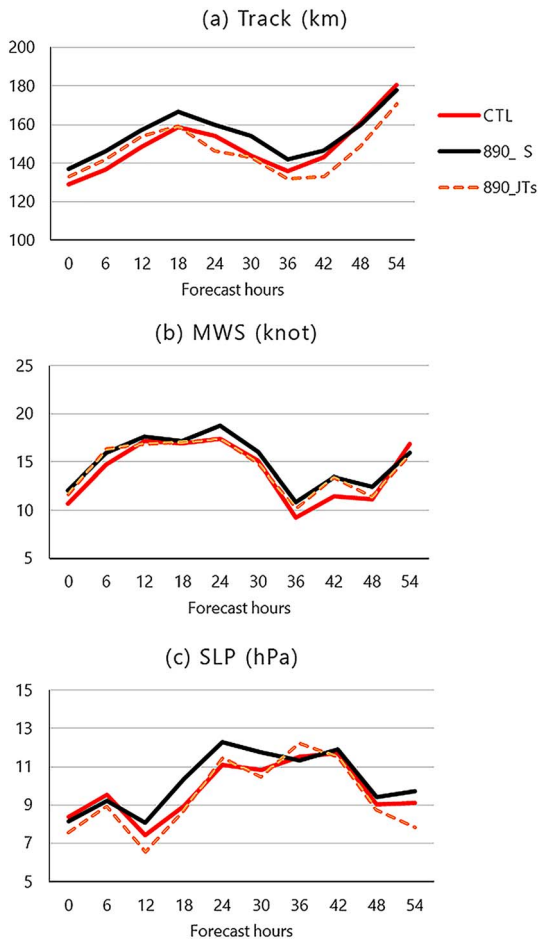
Figure 7. Root-mean-square errors of the (a) Hurricane Harvey track, (b) MWS, and (c) SLP forecasts according to the forecast hours. MWS = maximum 10-m wind speed; SLP = sea level pressure.

areas, J_{Ts} of Bands 9 and 10 are higher than those over the other areas. Hence, the high surface terrain affects not only Band 10 but also Bands 9 and 8.

In addition to the high-terrain areas, there are other areas where the values are greater than 0 K/K in Bands 8, 9, and 10. Figures 9e–9g illustrate when J_{Ts} is greater than 0 K, but with surface elevation points higher than 1,000 m removed. There are two locations with these characteristics: the Midwest and the eastern Pacific Ocean near the equator. All three bands show sensitivity to the surface. To further identify possible reasons for this anomaly, ABI Band 9 imagery is displayed in Figure 9d. The Band 9 imagery shows that the regions of elevated J_{Ts} in Figures 9e–9g are dry areas (dark color). Figure 9 indicates that water vapor bands may become sensitive to the surface when there is not enough moisture in the atmosphere, that is, high terrains, or dry areas.

Figures 9h–9j show histograms of J_{Ts} in Figures 9a–9c. The maximum J_{Ts} are 4.22991e−09 K/K, 0.000123885 K/K, and 0.0214650 K/K for Bands 8, 9, and 10, respectively. As expected, the greatest J_{Ts} are shown in Band 10 since Band 10 is closest to the surface. These are very small values, indicating the sensitivity of these three ABI spectral bands to the surface is minimal. However, as will be shown later, these small sensitivities pose substantial challenges to assimilating the radiance observations. This is due to four parameters involved in the inverse process during assimilation: temperature profile, moisture profile, surface skin temperature, and surface emissivity. Conversely, assimilating water vapor that is not sensitive to the surface is easier because the surface contributions are eliminated. Thus, the optimization of the ABI water vapor radiance assimilation will focus on quality control (QC), which eliminates the observations affected by the surface.

4.3. Handling Surface Impact for ABI Radiance Assimilation

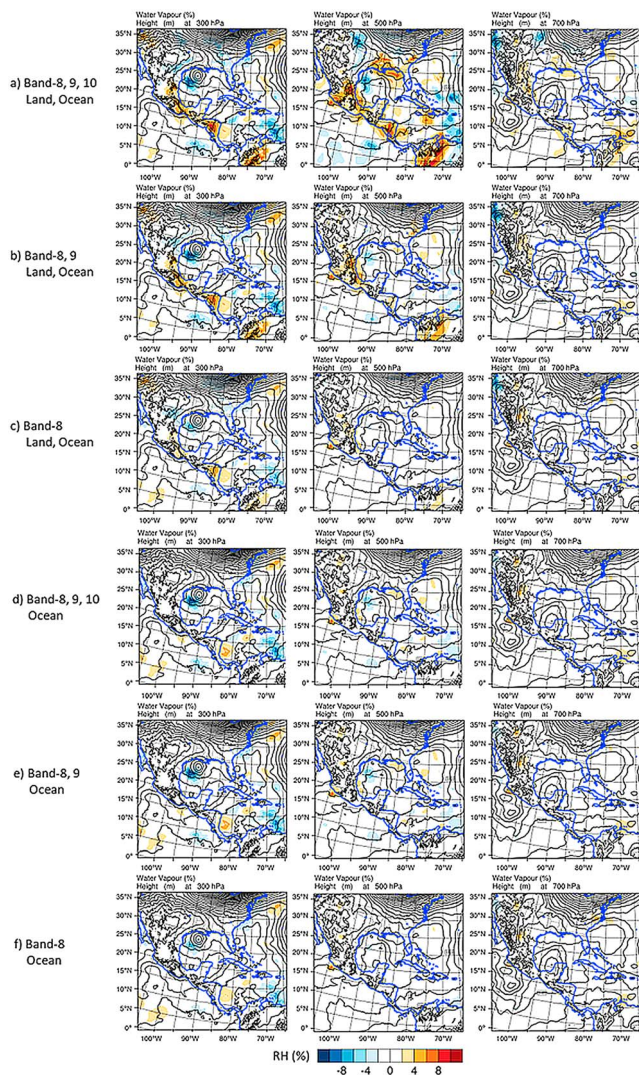As mentioned above, ABI water vapor band radiance assimilation can be negatively affected by the surface especially at higher elevations. The method of assimilating ABI radiances requires modification in order to reduce surface effects, especially for bands affected by terrain. For this purpose, additional experiments were conducted, and forecasting performances are analyzed in this section. Table 2 describes the data usage of the additional experiments on Hurricane Harvey (2017).

The 890_LS was previously conducted as EXP in section 3. Six more experiments were conducted by changing the band use and land/sea use (e.g., "89LS0S" uses Bands 8 and 9 over both land and sea and uses Band 10 only over sea). In addition, two more experiments were conducted limiting ABI radiance assimilation by the surface elevation, which removed ABI radiances when the elevation was greater than 500 m (89_H500) or 200 m (89_H200). These experiments will help determine an optimal method for assimilating ABI water vapor radiances.

In addition, J_{Ts} was employed as a QC parameter in the experiments since the surface impact from high surface terrain and dry atmosphere were identified by J_{Ts} as mentioned above. In this method, thresholds of J_{Ts} were set differently for each water vapor band based on the histogram (Figures 9h–9j) and the spatial distribution of J_{Ts}. The threshold values (Table 2) are empirically defined with consideration to minimizing surface impact while retaining data impact. Figure 10 shows the coverage of ABI radiances assimilated at 0600 UTC on 23 August 2017 in this study. The data points for the three ABI water vapor absorption bands in Figures 10a–10c are from the 890_LS, showing that nearly the same distribution of radiances are assimilated from each ABI band. After applying the threshold on J_{Ts} (Figures 10d–10f), many points were eliminated, which indicates that fewer ABI radiances were assimilated when possible contributions from the land surface are considered. For Band 8, comparably smaller amounts of data are removed (Figure 10d). The data

Figure 8. Relative humidity analysis field differences between the CTL and EXP (EXP − CTL) at 0600 UTC on 23 August 2017. (a) Bands 8, 9, and 10—land and ocean; (b) Bands 8 and 9—land and ocean; (c) Band 8—land and ocean; (d) Bands 8, 9, and 10—ocean; (e) Bands 8 and 9—ocean; (f) Band 8—ocean; RH = relative humidity; CTL = control run; EXP = experiments.

removed by applying the threshold on J_{Ts} increases in Band 9 (Figure 10e) and more increases in Band 10 (Figure 10f). Since Band 10 is the most sensitive to the surface, it makes sense that assimilating less radiance data from Band 10 would reduce the surface effect.

The initial time and other configurations for the additional experiments are consistent with 890_LS except for in the process of assimilating ABI radiances. The mean RMSEs of Hurricane Harvey's track, MWS, and SLP are calculated according to each forecast time from the analysis to 54-hr forecasts before Harvey's landfall. Finally, RMSE improvement rates (%) are calculated as below for the hurricane track, the MWS, and the SLP and are shown in Figure 11.

$$\text{RMSE improvement rate } (\%) = \frac{\text{RMSE of CTL} - \text{RMSE of EXP}}{\text{RMSE of CTL}} \times 100$$

The RMSE improvement rate is a percentage that indicates how much the hurricane forecast errors are decreased by assimilating ABI radiances. Positive and negative values in this figure refer to the improvement and degradation of the hurricane forecast performance, respectively.

The RMSE improvement rates of the 890_LS are all negative for the hurricane track, the MWS, and the SLP, which is consistent from the RMSEs in Figure 7. By removing the lowest level band (10), which is more prone to surface contribution than the other two bands, the track forecast errors are improved in the 89_LS, 89_S, and 8LS_9S. Removing ABI radiances over land in the 890_S improved track and SLP forecasts.

The experiments eliminating ABI radiances over high surface terrain such as the 89_H500 and 89_H200 reduced the forecast errors as well. In the 89_H200, ABI radiances with the surface elevation less than 200 m were assimilated, which improved the hurricane forecast track greater than 3.1%, and the MWS by about 1.5%. Including more data by relaxing surface elevations up to 500 m (89_H500 more ABI radiances over high surface than the 89_H200) results in an increase in hurricane track errors and a decrease in the RMSEs of the SLP. It shows, in this case, that the surface impact is increased due to assimilating more radiance data over the high surface terrain.

The analysis from the experiments indicates that the assimilation benefits from the elimination of certain observations that might be prone to surface contributions, such as Band 10, or observations over land or observations wi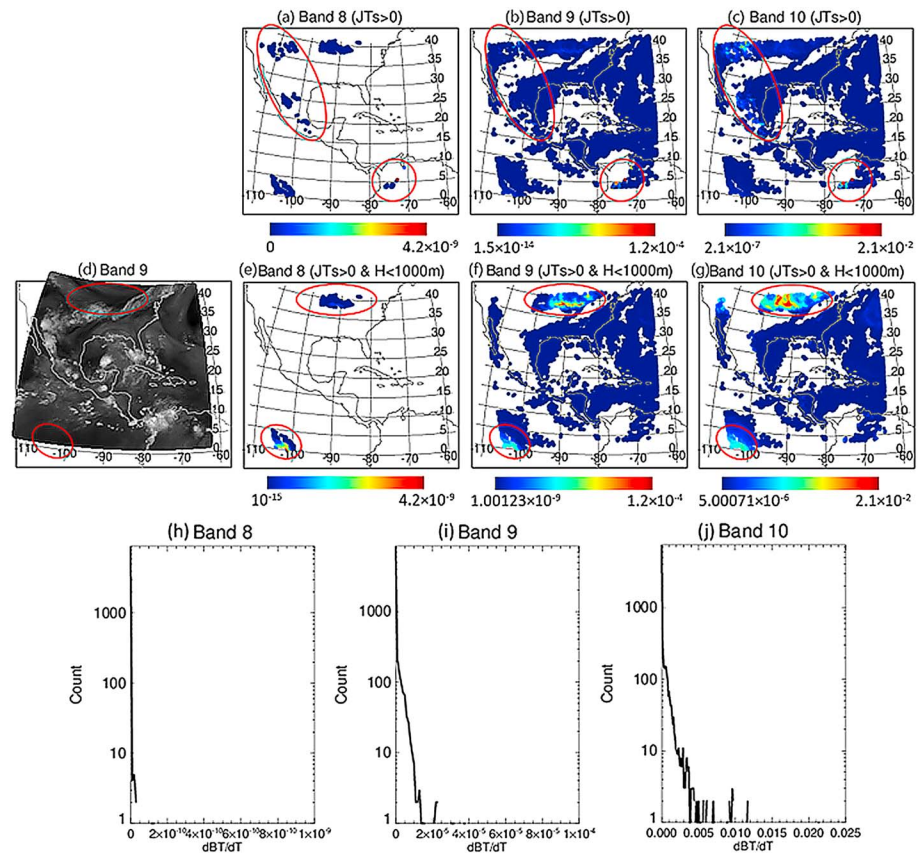th surface elevations greater than a certain value. However, eliminating too many observations would result in too few observations assimilated, which could lead to reduced positive impact or even negative impact. Therefore, an objective method is needed to eliminate observations affected by the surface and retain observations not affected by the surface. This idea can be realized by using skin temperature Jacobians as a QC parameter. This method is superior to other experiments because surface sensitivity is associated with many factors, such as surface type, surface elevation, and moisture content. But none of these factors can be used alone to discriminate observations affected by the surface from those that are not. Further, the discrimination is complicated by one often overlooked factor: the viewing angle. A narrow viewing angle is more likely affected by the surface than a wider angle when surface types, surface elevation, and moisture content are constant. The Jacobian of surface skin temperature, when considering all factors, objectively quantifies the sensitivity of the radiance to the surface.

From Figure 11, the experiment of 890_JTs appears to have the largest overall RMSE improvement rate among all experiments; both the track and the SLP are improved by 3.6% and 4.3%, respectively, with no significant impact on the MWS (also in Figure 7). When dropping Band 10, the track forecast of the 89_JTs is

Figure 9. Jacobian functions of skin temperature (J_{Ts}) at 0600 UTC on 23 August 2017. (a, b, and c) The plots when J_{Ts} is above 0 K, and (e, f, and g) the plots when J_{Ts} is above 0 K and the surface height is less than 1,000 m. (h, i, and j) Histograms of J_{Ts}. (d) the Advanced Baseline imager Band 9 imagery.

improved about 5.8%, and the MWS RMSEs are reduced by 1.1%, although the SLP is degraded by 7.5%, compared to the CTL. These results indicate that more water vapor radiances from multiple bands assimilated are beneficial to the Hurricane Harvey forecast, but it is critical to eliminate those observations affected by the surface before assimilation.

Table 2
Description of the Additional Experiments for ABI Radiance Assimilation on Hurricane Harvey (2017)

	Data used in CTL: CONV, AMSUA, ATMS, IASI, CrIS (including CCRs)	ABI radiance		
		Band 8	Band 9	Band 10
890_LS	√	Land/sea	Land/sea	Land/sea
89_LS	√	Land/sea	Land/sea	×
890_S	√	Sea	Sea	Sea
89_S	√	Sea	Sea	×
89LS0S	√	Land/sea	Land/sea	Sea
8LS90S	√	Land/sea	Sea	Sea
8LS9S	√	Land/sea	Sea	×
89_H500	√	Height < 500 m	Height < 500 m	×
89_H200	√	Height < 200 m	Height < 200 m	×
890_JTs	√	$J_{Ts} = 0$	$J_{Ts} < 10^{-9}$	$J_{Ts} < 5 \times 10^{-6}$
89_JTs	√	$J_{Ts} = 0$	$J_{Ts} < 10^{-9}$	×

Note. ABI = Advanced Baseline imager. CTL = control; CONV = conventional observations; AMSU-A = Advanced Microwave Sounding Unit; ATMS = Advanced Technology Microwave Sounder; IASI = Infrared Atmospheric Sounding Interferometer; CrIS = Cross-track Infrared Sounder; CCRs = Cloud-Cleared radiances.
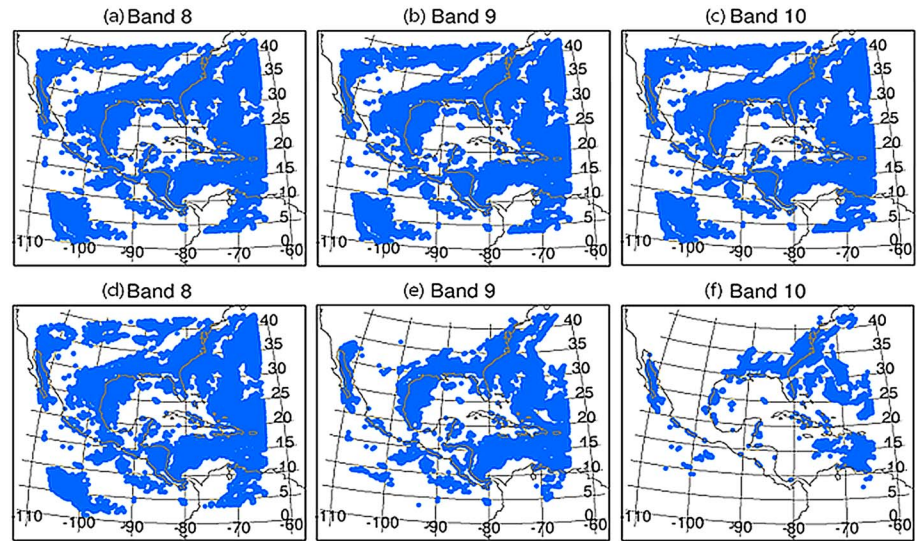
Figure 10. The coverage plots of Advanced Baseline imager radiances assimilated before (a–c) and after applying threshold on J_{T_s} (d–f) at 0600 UTC on 23 August 2017.

Figure 12 shows the relative humidity analysis difference between the CTL and EXP at 1200 UTC on 24 August 2017 which is in the middle of the Hurricane Harvey forecast period. As expected from Figure 8a, continuous assimilation of three bands over land and ocean (890_LS) significantly increases the water vapor content in the model field by more than 20% in relative humidity in some regions. This is likely due to the assimilation of surface-affected water vapor radiances. Conversely, the moisture increment in the 890_JTs, which removes all surface affected radiances, is significantly decreased and leads to improved forecasts in track and SLP for Hurricane Harvey.

It is important to note that the J_{T_s} threshold is most effective when there are sufficient observations affected by the surface. If the atmosphere is moist enough, all radiances can be assimilated, as displayed in Figure 5 for Hurricane Irma. There are no significant differences between the results of 890_LS and 890_JTs (also in Figure 4). The RMSEs of track, MWS, and SLP are similar to all of the forecast hours, except the last 12 hr, where only small differences are seen. This is due to the minimal surface impact for Hurricane Irma since
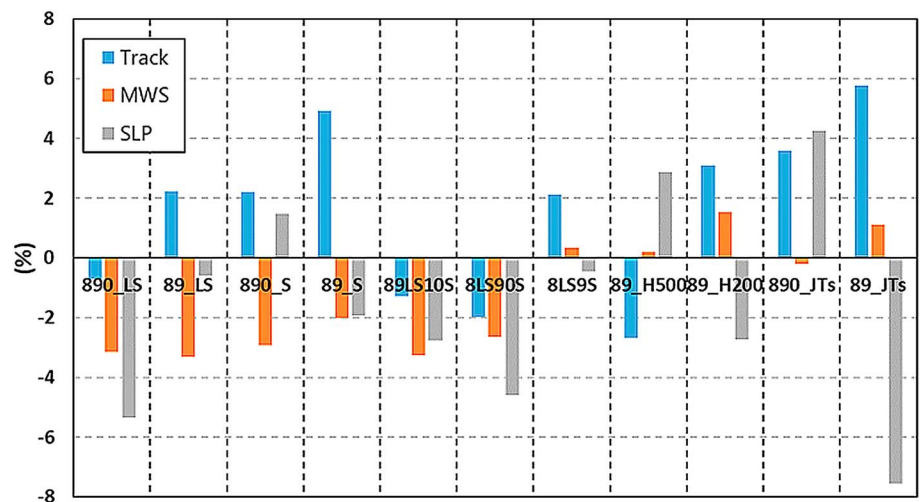

Figure 11. The root-mean-square error improvement rates of the additional experiments in Table 2. Positive values indicate positive impact of Advanced Baseline imager radiance assimilation. MWS = maximum 10-m wind speed; SLP = sea level pressure.
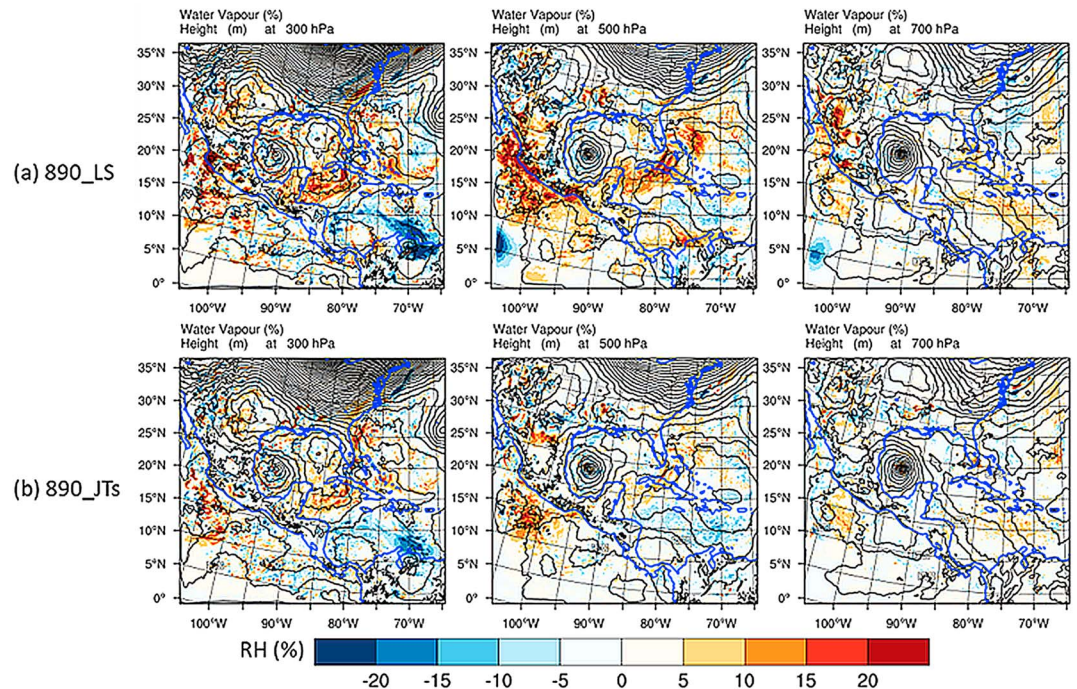
Figure 12. The analysis difference images of the relative humidity between CTL and EXP (EXP − CTL) at 1200 UTC on 24 August 2017 from the experiments (a) 890_LS and (b) 890_JTs. RH = relative humidity; CTL = control run; EXP = experiments.

fewer ABI radiances are removed. Most of the radiances that have been removed are from dry regions and at greater distances from the hurricane.

Through the comparisons of these experiments, it is shown that ABI water vapor band radiance assimilation can be improved by appropriately handling the surface impact. It is true that water vapor band radiance assimilation could be improved to some extent by eliminating certain types of radiance observations (e.g., Band 10 radiances, or radiances over land). However, useful information could be lost by discarding the entire data set. From our experiments above, employing surface skin temperature Jacobian (J_{Ts}) as an objective parameter to determine the surface impact is because it can successfully remove all surface affected radiances, whether it is due to high terrain, dry air, or large viewing angle in the ABI water vapor radiance assimilation.

5. Summary

The three water vapor bands of ABI on board GOES-16 provide moisture information from the lower to upper troposphere. The high temporal and spatial resolution of these observations can be helpful in improving high-impact weather forecasts. In this study, the radiances from the three water vapor bands of GOES-16 ABI were assimilated through a GSI data assimilation system in the WRF-ARW model, and the forecast impacts for Hurricane Irma (2017) and Hurricane Harvey (2017) have been studied and analyzed. The track RMSE of Hurricane Irma (2017) forecasts is reduced up to 108 km in the 84-hr forecast by assimilating ABI radiances from the three water vapor bands over both land and sea.

By comparison, Hurricane Harvey (2017) showed negative impacts on both track and intensity forecasts when all three water vapor band radiances were assimilated over land and sea. In the Harvey case, some of the radiances are affected by surface contributions, that is, over high terrains or when the atmosphere is relatively dry. The complication of surface contamination increases the number of unknowns in the inverse process in assimilation and degrades the accuracy of the analysis. Therefore, additional QC is needed in order to eliminate the observations affected by the surface. To better understand the surface impact, different approaches have been tested to remove the overwhelming contribution from the surface in the water vapor radiance assimilation. They include (1) removing lower-level sensitive channels (Band 10); (2)

removing radiances over land; and (3) limiting the surface elevation to remove radiances over the high surface (500 or 200 m). These approaches may reduce the surface effect and improve the analysis and forecasts; however, discarding an entire subset of data could result in the loss of unaffected useful data and minimize, or prevent, any improvements in analysis.

An objective approach is needed to determine which radiance observation is affected or not affected by the surface. The surface skin temperature Jacobian, J_{Ts}, is well suited as such an objective QC parameter. It will eliminate radiance observations with surface contributions in an objective and quantitative way and retain all useful information (not affected by the surface). It can remove not only the negative effects of the high terrain areas but also the sensitivity of the dry areas in the ABI radiance assimilation. Further, it accounts for the viewing angle. With the objective QC of J_{Ts}, both track and intensities are improved for the Hurricane Harvey (2017) forecasts, while the forecast RMSEs of the track and SLP are decreased by 3.6% and 4.3%, respectively, when all three water vapor bands radiances (not affected by surface) are assimilated.

The same J_{Ts} method is also applied to Hurricane Irma, which has already shown substantial improvement in track forecast without any QC to eliminate surface impact. The further improvement from the J_{Ts} QC is not obvious, and the RMSEs of track and intensity forecast remain mostly unchanged. In contrast to Hurricane Harvey, Hurricane Irma forecasts involved fewer radiance observations that were affected by surface contributions. The J_{Ts}-based QC rejects far fewer radiance observations from assimilation. These results indicate that J_{Ts} can be an objective QC parameter used in regular assimilation to eliminate surface impact without limiting other types of control factors such as land surface or special bands. This is critically important for assimilating absorption band radiances because it simplifies the inverse problem in assimilation by eliminating the unknowns of surface skin temperature and surface emissivity. The J_{Ts} has the potential to enhance the forecasts of other atmospheric phenomena beyond TCs. This method might prove to be particularly useful for weather systems that are not as moist as TCs due to the likelihood of greater surface contributions. This method can be applied to global NWP models where a wide range of weather phenomena are expected, and it can also be applied to assimilate water vapor radiances from other sensors on board geostationary satellites and polar orbiting satellites. Moreover, the application is not limited to water vapor radiances in the IR but includes microwave as well. For future works, sensitivity study on thinning size or cloud masking method could be examined for the optimal assimilation of the three water vapor bands of ABI.

References

Blake, E. S. & Zelinsky, D. A. (2018). Hurricane Harvey (AL092017) 17 August–1 September 2017, Tropical Cyclone Report, 1-77.

Cangialosi, J. P., Latto, A. S. & Berg, R. (2018), Hurricane Irma (AL112017) 30 August–12 September 2017, Tropical Cyclone Report, 1-111.

Chen, Y., Han, Y., Delst, P. V., & Weng, F. (2010). On water vapor Jacobian in fast radiative transfer model. *Journal of Geophysical Research*, *115*, D12303. https://doi.org/10.1029/2009JD013379

Chen, Y., Han, Y., & Weng, F. (2012). Comparison of two transmittance algorithms in the community radiative transfer mode: Application to AVHRR. *Journal of Geophysical Research*, *117*, D06206. https://doi.org/10.1029/2011JD016656

Hong, S.-Y., & Lim, J.-O. J. (2006). The WRF single-moment 6-class microphysics scheme (WSM6). *Journal of the Korean Meteorological Society*, *42*, 129–151.

Hong, S.-Y., Noh, Y., & Dudhia, J. (2006). A new vertical diffusion package with an explicit treatment of entrainment processes. *Monthly Weather Review*, *134*(9), 2318–2341. https://doi.org/10.1175/MWR3199.1

Hu, M., Ge, G., Shao, H., Stark, D., Newman, K., Zhou, C., et al. (2017). Grid-point Statistical Interpolation (GSI) user's guide version 3.6. Developmental Testbed Center. Available at http://www.dtcenter.org/com-GSI/users/docs/index.php, 150 pp.

Iacono, M. J., Delamere, J. S., Mlawer, E. J., Shephard, M. W., Clough, S. A., & Collins, W. D. (2008). Radiative forcing by long-lived greenhouse gases: Calculations with the AER radiative transfer models. *Journal of Geophysical Research*, *113*, D13103. https://doi.org/10.1029/2008JD009944

Kain, J. S. (2004). The Kain-Fritsch convective parameterization: An update. *Journal of Applied Meteorology and Climatology*, *43*, 170–181. https://doi.org/10.1175/1520-0450(2004)043<0170:TKCPAU>2.0.CO;2

Li, J., Liu, C. Y., Huang, H.-L., Schmit, T. J., Menzel, W. P., & Gurka, J. (2005). Optimal cloud-clearing for AIRS radiances using MODIS. *IEEE Transactions on Geoscience and Remote Sensing*, *43*, 1266–1278.

Li, J., Wang, P., Han, H., Li, J., & Zheng, J. (2016). On the assimilation of satellite sounder data in cloudy skies in the numerical weather prediction models. *Journal of Meteorological Research*, *30*(2), 169–182. https://doi.org/10.1007/s13351-016-5114-2

Lu, J., Feng, T., Li, J., Cai, Z., Xu, X., Li, L., & Li, J. (2019). Impact of assimilating Himawari-8 derived layered precipitable water with varying cumulus and microphysics parameterization schemes on the simulation of Typhoon Hato. *Journal of Geophysical Research: Atmospheres*, *124*, 3050–3071. https://doi.org/10.1029/2018JD029364

Ma, Z., Maddy, E. S., Zhang, B., Zhu, T., & Boukabara, S. A. (2017). Impact assessment of Himawari-8 AHI data assimilation in NCEP GDAS/GFS with GSI. *Journal of Atmospheric and Ocean Technology*, *34*(4), 797–815. https://doi.org/10.1175/JTECH-D-16-0136.1

Min, M., Wu, C., Li, C., Liu, H., Xu, N., Wu, X., et al. (2017). Developing the science product algorithm testbed for Chinese next-generation geostationary meteorological satellites: Fengyun-4 series. *Journal of Meteorological Research*, *31*(4), 708–719. https://doi.org/10.1007/s13351-017-6161-z

Moody, J. L., Wimmers, A. J., & Davenport, J. C. (1999). Remotely sensed specific humidity: Development of a derived product from the GOES Imager channel 3. *Geophysical Research Letters*, *26*(1), 59–62. https://doi.org/10.1029/1998GL900222

Qin, Z., Zou, X., & Weng, F. (2013). Evaluating added benefits of assimilating GOES imager radiance data in GSI for coastal QPFs. *Monthly Weather Review*, *141*(1), 75–92. https://doi.org/10.1175/MWR-D-12-00079.1

Qin, Z., Zou, X., & Weng, F. (2017). Impacts of assimilating all or GOES-like AHI infrared channels radiances on QPFs over Eastern China. *Tellus*, *69*(1). https://doi.org/10.1080/16000870.2017.1345265

Realmuto, V. J., Sutton, A. J., & Elias, T. (1997). Multispectral thermal infrared mapping of sulfur dioxide plumes: A case study from the East Rift Zone of Kilauea Volcano, Hawaii. *Journal of Geophysical Research*, *102*(B7), 15,057–15,072. https://doi.org/10.1029/96JB03916

Schmit, T. J., Griffith, P., Gunshor, M. M., Daniels, J. M., Goodman, S. K., & Lebair, W. K. (2017). A closer look at the ABI on the GOES-R series. *Bulletin of the American Meteorological Society*, *98*(4), 681–698. https://doi.org/10.1175/BAMS-D-15-00230.1

Schmit, T. J., Gunshor, M. M., Menzel, W. P., Gurka, J. J., Li, J., & Bachmeier, A. S. (2005). Introducing the next-generation Advanced Baseline Imager (ABI) on GOES-R. *Bulletin of American Meteorological Society*, *86*(8), 1079–1096. https://doi.org/10.1175/BAMS-86-8-1079

Skamarock, W. C., Klemp, J. B., Dudhia, J., Gill, D. O., Barker, D. M., Duda, M. G., et al. (2008). A description of the Advanced Research WRF version 3. NCAR Technical Note NCAR/TN475 + STR, 113 pp., doi:https://doi.org/10.5065/D68S4MVH

Soden, B. J., & Bretherton, F. P. (1993). Upper tropospheric relative humidity from the GOES 6.7 μm channel: Method and climatology for July 1987. *Journal of Geophysical Research*, *98*(D9), 16,669–16,688. https://doi.org/10.1029/93JD01283

Wang, P., Li, J., Goldberg, M. D., Schmit, T. J., Lim, A. H. N., Li, Z., et al. (2015). Assimilation of thermodynamic information from advanced IR sounders under partially cloudy skies for regional NWP. *Journal of Geophysical Research: Atmospheres*, *120*, 5469–5484. https://doi.org/10.1002/2014JD022976

Wang, P., Li, J., Li, J., Li, Z., Schmit, T. J., & Bai, W. (2014). Advanced infrared sounder subpixel cloud detection with imagers and its impact on radiance assimilation in NWP. *Geophysical Research Letters*, *41*, 1773–1780. https://doi.org/10.1002/2013GL059067

Wang, P., Li, J., Li, Z., Lim, A. H. N., Li, J., Schmit, T. J., & Goldberg, M. D. (2017). The impact of Cross-track Infrared Sounder (CrIS) cloud-cleared radiances on Hurricane Joaquin (2015) and Matthew (2016) forecasts. *Journal of Geophysical Research: Atmospheres*, *122*, 13,201–13,218. https://doi.org/10.1002/2017JD027515

Wang, P., Li, J., Lu, B., Schmit, T. J., Lu, J., Lee, Y.-K., et al. (2018). Impact of moisture information from advanced Himawari imager measurements on heavy precipitation forecasts in a regional NWP model. *Journal of Geophysical Research: Atmospheres*, *123*, 6022–6038. https://doi.org/10.1029/2017JD028012

Weldon, R. B., & Holmes, S. J. (1991). Water vapor imagery—Interpretation and applications to weather analysis and forecasting, NOAA Technical Reports NESDIS 57, 213 pp.

Yang, J., Zhang, Z., Wei, C., Lu, F., & Guo, Q. (2017). Introducing the new generation of Chinese geostationary weather satellites, Fengyun-4. *Bulletin of the American Meteorological Society*, *98*(8), 1637–1658. https://doi.org/10.1175/BAMS-D-16-0065.1

Zhu, Y., Derber, J., Collard, A., Dee, D., Treadon, R., Gayno, G., & Jung, J. A. (2014). Enhanced radiance bias correction in the National Centers for Environmental Prediction's Gridpoint Statistical Interpolation data assimilation system. *Quarterly Journal of the Royal Meteorological Society*, *240*(682), 1479–1492.

Zou, X., Qin, Z., & Weng, F. (2011). Improved coastal precipitation forecasts with direct assimilation of GOES-11/12 imager radiances. *Monthly Weather Review*, *139*(12), 3711–3729. https://doi.org/10.1175/MWR-D-10-05040.1